



Pink-beam focusing with a one-dimensional compound refractive lens

Eric M. Dufresne,* Robert W. Dunford, Elliot P. Kanter, Yuan Gao, Seoksu Moon, Donald A. Walko and Xusheng Zhang

Argonne National Laboratory, 9700 South Cass Avenue, Argonne, IL 60439, USA.

*Correspondence e-mail: dufresne@anl.gov

Received 16 March 2016

Accepted 8 June 2016

Edited by G. E. Ice, Oak Ridge National Laboratory, USA

Keywords: compound refractive lenses; pink beam; chromatic aberration.

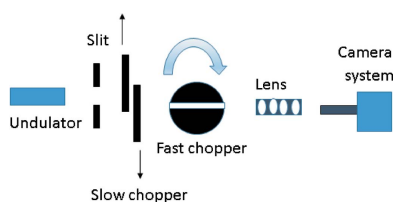
The performance of a cooled Be compound refractive lens (CRL) has been tested at the Advanced Photon Source (APS) to enable vertical focusing of the pink beam and permit the X-ray beam to spatially overlap with an 80 μm -high low-density plasma that simulates astrophysical environments. Focusing the fundamental harmonics of an insertion device white beam increases the APS power density; here, a power density as high as 500 W mm^{-2} was calculated. A CRL is chromatic so it does not efficiently focus X-rays whose energies are above the fundamental. Only the fundamental of the undulator focuses at the experiment. A two-chopper system reduces the power density on the imaging system and lens by four orders of magnitude, enabling imaging of the focal plane without any X-ray filter. A method to measure such high power density as well as the performance of the lens in focusing the pink beam is reported.

1. Introduction

Following plasma physics experiments designed to simulate astrophysical environments with an electron beam ion trap (EBIT) (Silver *et al.*, 2011), it was found that a broad band source of X-rays with a few percent bandwidth could provide an enhanced signal over a monochromatic beam. A ‘pink’ beam generated from the first harmonic of an undulator from a third-generation synchrotron source can provide this capability. As the EBIT generates a plasma that is 80 μm tall, the pink X-ray beam must spatially overlap with the plasma. Beams at third-generation synchrotrons are typically a few millimetres wide; thus, the pink beam must be focused to achieve efficient overlap.

Focused pink beams can be produced typically with figured grazing-incidence mirrors or multilayer monochromators. Another approach would be to use a compound refractive lens (CRL) (Snigirev *et al.*, 1996), although they have strong chromatic aberrations. This has been used advantageously recently to reduce the harmonic content of a monochromatic beam (Polikarpov *et al.*, 2014). The experimenters used a slit to spatially filter focused X-rays of the fundamental energy from the unfocused higher harmonics. The higher harmonics were reduced by a factor of 1000 in the flux measured after the slit (Polikarpov *et al.*, 2014).

Recent progress has been made in simulations of refractive lenses with ray-tracing methods like *SHADOW* (Alianelli *et al.*, 2007). The authors, for example, simulated polychromatic focusing with Be lenses of a 40%-wide energy band centered around 12 keV. Chromatic aberrations were significant in this example. If the energy spectrum of the first harmonic line has a few-percent-wide bandpass, the chromatic



aberration can remain small. To our knowledge, the performance of a CRL to focus a pink beam at high demagnification has not been reported to date. Also, simple expressions to estimate the focal spot size that includes chromatic aberrations are not readily available in the literature. We thus have tested the performance of a cooled Be CRL in the Advanced Photon Source (APS) 7-ID-B hutch to enable vertical focusing of the pink beam in that hutch and to permit the X-ray beam to spatially overlap with an 80 μm -high low-density plasma. This paper provides some estimates of the chromatic aberration expected from such a pink beam, describes the technique employed to measure a focused beam with large power density and finally shows some typical results obtained at two photon energies.

2. Theory

The focal length of a parabolic compound refractive lens is given by

$$f = \frac{R}{2N\delta}, \quad (1)$$

where R is the radius of curvature of a lenslet, N is the number of lenslets and δ is the index of refraction decrement (Snigirev *et al.*, 1996; Lengeler *et al.*, 2002). Refractive lenses have strong chromatic aberration due to the energy dependence of $\delta \propto 1/E^2$. Nevertheless, for a small energy band such as the natural width of an undulator harmonics, $\Delta E/E \approx 1/N_p$, where N_p is the number of periods of the undulator, these aberrations may be acceptable and provide an adequate focus for an experiment. For the APS standard undulator A, $\Delta E/E \approx 2\text{--}3\%$, depending on the white-beam beam size at the lens (see Fig. 1).

To estimate the chromatic aberration in an experiment where the source–lens distance $r_s \gg f$, we expect the root-mean-square (RMS) focal spot size to be $\sigma_i = \sigma_s r_i / r_s \approx f \sigma_s / r_s$, where σ_s is the RMS source size, and r_i is the lens–image plane distance. For a pink beam with a

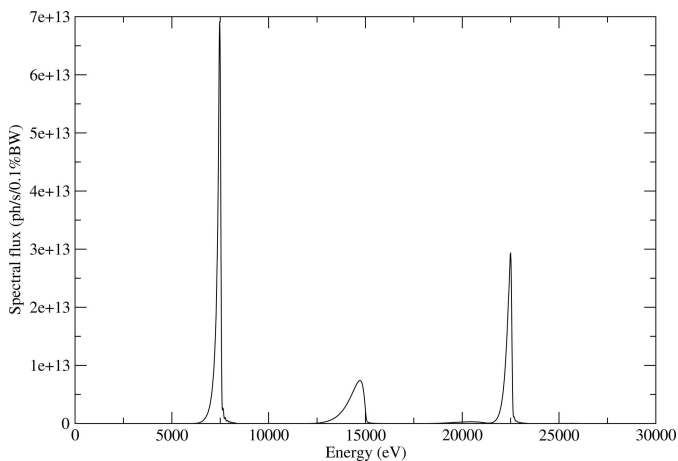


Figure 1
Calculated spectral flux through the white-beam slits with a fundamental peak set at 7.47 keV. The FWHM of the first harmonic is 2.2%. The second and third harmonics are also seen above 10 keV.

Table 1

Expected spot size from simple theoretical estimate, computing σ_E/E from standard X-ray source simulations (or assuming it to be equal to 1%).

Energy (keV)	N	f (m)	δ	l (mm)	σ_E/E (%)	σ_a (μm)	σ_i (μm)	σ_{ip} (μm)
6.1	4	3.3	9.178×10^{-6}	2.46	0.84	273	1.08	4.7
7.47	6	3.3	6.117×10^{-6}	4.75	0.92	310	1.08	5.8
9.97	10	3.3	3.432×10^{-6}	12.2	1	372	1.08	7.5

Gaussian spectral and spatial profile, we use the energy dependence of δ to show that the focal length now has an RMS deviation of $\sigma_f \approx (2\sigma_E/E)f$, where σ_E is the RMS energy spread of the undulator harmonics used. Due to this energy variation, the beam size at the focal length for the peak of the spectra is broadened by a factor $\text{NA} \times \sigma_f$, where the numerical aperture of the lens $\text{NA} = \sigma_a/f$. Typically the physical aperture of a refractive lens,

$$\sigma_a = (f\delta l)^{1/2}, \quad (2)$$

is limited by the absorption length l , and the properties and geometry of the material. Equation (2) is the RMS standard deviation of the Gaussian transmission profile of the CRL. We assume this profile here to be semi-infinite. For simplicity, we ignored the case where the NA is limited by an aperture comparable to σ_a . Adding this latter broadening in quadrature with σ_i , we expect the pink beam focal spot size to be

$$\sigma_{ip} \approx [\sigma_i^2 + (2\sigma_a\sigma_E/E)^2]^{1/2}. \quad (3)$$

Table 1 shows the expected broadening from focusing a pink beam. Here $R = 0.2$ mm, $\sigma_s = 11.6$ μm , $r_s = 35.5$ m, and σ_E/E is derived from X-ray optical simulations using the software package *XOP* (Sanchez del Rio & Dejus, 1997) shown in Fig. 1. The rough estimate of the focal spot size of the pink beam is significantly larger than σ_i , but remains in this example below 10 μm . This beam size would suit many modern synchrotron experiments and is adequate for the proposed EBIT experiment.

A similar expression can be derived for arbitrary magnification ratios from the energy dependence of the image distance $r_i = r_s f / (r_s - f)$, derived using the thin-lens formula. Then the RMS spot size with pink beam is

$$\sigma_{ip} \approx \left\{ \sigma_i^2 + \left[2 \frac{r_s^2}{(r_s - f)^2} \frac{f}{r_i} \sigma_a \sigma_E/E \right]^2 \right\}^{1/2}. \quad (4)$$

Equation (4) reduces to equation (3) when $f \ll r_s$.

The dependence of equation (4) is shown in Table 2 for 6.1 keV, for several r_i and $r_s = 35.5$ m. The expected spot size is closest to the demagnified source size at a magnification of 1:1 and is negligible for the same magnification when $\sigma_E/E \leq 0.001$.

If an entrance slit set to an opening $\Delta \ll \sigma_a$ limits the numerical aperture, one can rewrite equation (4) by replacing σ_a with $\Delta/2$. This may be helpful, for example, when one wants to filter the transverse coherent fraction of the source by setting Δ to a dimension smaller than the transverse coher-

Table 2

Ratio of the expected spot size σ_{ip} over the demagnified image of the source σ_i from equation (4) for different relative bandwidth and r_i .

σ_E/E	r_i (m)	σ_{ip}/σ_i
0.01	3.64	5.16
0.01	4.44	4.74
0.01	7.1	3.91
0.01	8.88	3.59
0.01	11.83	3.25
0.01	17.75	2.85
0.01	35.5	2.40
0.001	35.5	1.023
0.0001	35.5	1.00024

ence length of the source. With coherent illumination, one would also add a diffraction-limited spot size component of $\sigma_d = 0.377\lambda r_i/\Delta$ in quadrature with σ_i in equation (4).

3. Experimental method

The experimental setup is shown in Fig. 2. This experiment was performed on the 7-ID beamline of the APS, in the white-beam enclosure 7-ID-B. A standard undulator A (72 periods of 33 mm) produced white beam with a power density as high as 250 W mm^{-2} . At this power density, scintillator crystals such as YAG:Ce used for viewing intense X-rays will crack and melt. As they heat up, their light output will also drop. However, it is possible to use a YAG:Ce scintillator in phase-contrast imaging experiments if the duration of the X-ray beam is reduced to less than 10 ms (Reeves *et al.*, 2009). The APS bunch pattern for this experiment was a uniformly filled bunch pattern with a repetition rate of 88 MHz. To reduce the heating power, the X-ray beam was gated by two mechanical shutters: a slow shutter operating at 1 Hz frequency with 10 ms opening duration and a fast shutter operating at 1 kHz frequency with 9 μs opening duration (Moon *et al.*, 2010).

The slow chopper uses two water-cooled copper blocks driven by a solenoid (see Fig. 2). The fast chopper (Gembicky *et al.*, 2005) is based on a fast spinning wheel mounted on an air bearing and powered by a servo motor that is phase-locked to the ring revolution frequency. Synchronized operation of these two shutters cuts off more than 99.99% of the incident beam power. The fast chopper rotation axis is perpendicular to the X-ray propagation direction. Two openings on the rims of the wheel reduce the X-ray repetition rate to 1 kHz. The two openings in this geometry work together to reduce the opening time by a factor of two (Gembicky & Coppens, 2007).

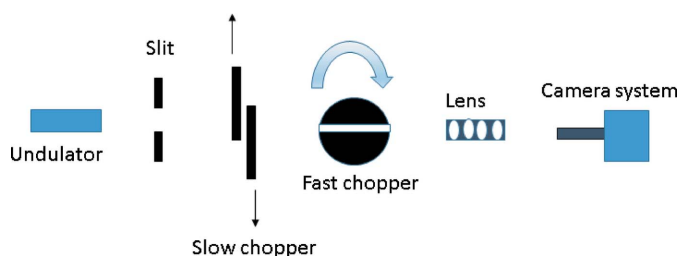


Figure 2
Side view of the experimental setup.

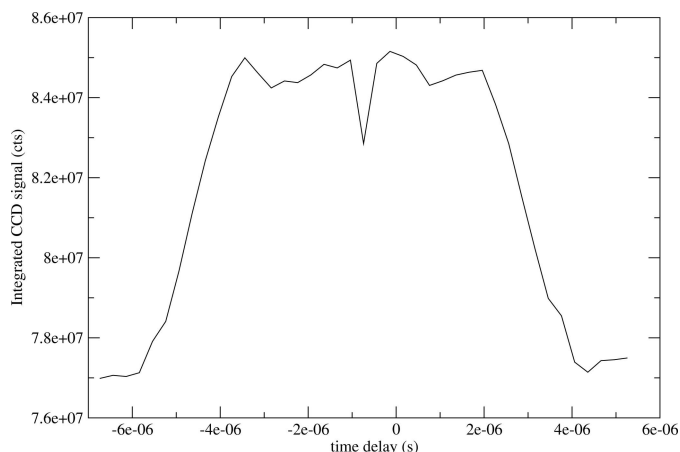


Figure 3
Timing overlap of the camera gate and the fast chopper window.

Fig. 3 shows the time delay scan between the CCD camera trigger and the fast X-ray chopper clock. The vertical opening of the chopper is 2.54 mm, so for a wheel with a 70 mm radius rotating at 500 Hz one expects an opening of $5.78 \mu\text{s}$. The top of the trapezoidal shape in Fig. 3 is consistent with this duration. The FWHM of the transmitted flux in Fig. 3 is about $8 \mu\text{s}$, so for a 10 ms slow chopper opening, with a 1 Hz frequency, the transmission is about 80 p.p.m. Note that the CCD data were not dark-subtracted, thus the chopper transmission when the beam is blocked appears artificially high.

White-beam slits placed 26.5 m from the source were set to an opening of 0.2 mm horizontally by 0.48 mm vertically. The vertical opening was set to prevent white beam from hitting the Cu lens mount. The lens was housed in a vacuum chamber in 7-ID-B 35.5 m from the source, and held by a water-cooled copper mount equipped with computer-controlled translation and rotation axes enabling the alignment of the lens (two transverse translation axes, a pitch and yaw axis of rotation). The mechanical assembly (from JJ X-ray, CRL-UHV cooled) enabled three separate combinations of lenses, which for these studies were $N = 4, 6$ and 10 .

The white X-rays were imaged by the visible fluorescence of either a LYSO:Ce or a YAG:Ce single-crystal screen, 3.3 m from the lens. The visible image was observed with a charge-coupled device (CCD) Sensicam camera from Cooke with 1376×1040 pixels each $6.4 \mu\text{m}$ coupled to a 5X Mitutoyo Apochromat objective and a 1X tube lens. Because of its longer X-ray absorption length, YAG:Ce is preferable to LySO:Ce for the white-beam experiments, as it can better tolerate the heat load. Using YAG:Ce reduces the spatial resolution of the detector owing to the long X-ray fluorescence path overlapping with the imaging system depth of focus. The LYSO:Ce single-crystal screen was used for monochromatic beam experiments.

4. Results

The focusing properties of the one-dimensional lenses were first tested with a monochromatic beam from a diamond (111) double-crystal monochromator set around 10 keV. This

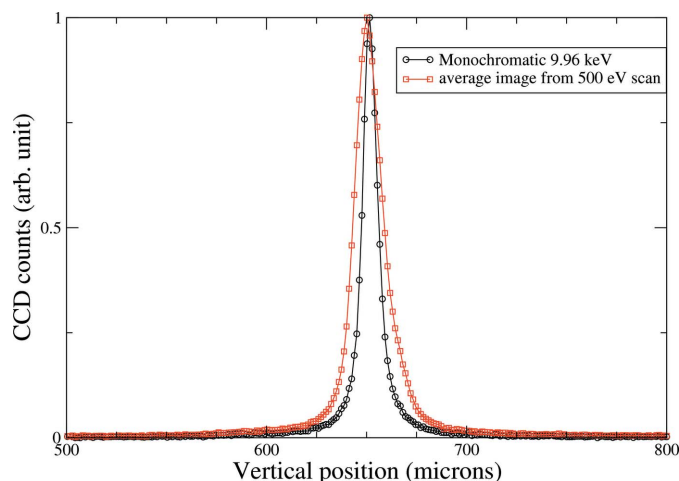


Figure 4
Monochromatic beam focus and averaged image from a 500 eV energy scan centered around 10 keV, to simulate a focused pink beam.

monochromator is housed 30 m from the source after the white-beam slits and its performance has been described elsewhere (Dufresne *et al.*, 2010). Fig. 4 shows the best monochromatic beam vertical focus at 9.96 keV, as well as an average of 51 images measured in 500 eV-wide energy scans of the monochromator from 9.66 to 10.16 keV to mimic pink-beam conditions. The average and single images have FWHM of 16.1 and 8.6 μm , respectively. The simulated pink beam performance compares well to the estimate shown in Table 1, *i.e.* a FWHM of 17.6 μm . We attribute the difference between the expected focal spot size with monochromatic conditions (2.5 μm) and our measurement in Fig. 4 to aberrations from the monochromator crystals and the Be lens.

Fig. 5 shows the optimized pink-beam focal spot of the vertical one-dimensional focusing lens with $N = 4$ at 6.1 keV. Using equation (1) and δ from Table 1, we find $f = 2.72$ m and $r_i = 2.95$ m, in good agreement with the experimental conditions. The best focus was found by scanning the undulator

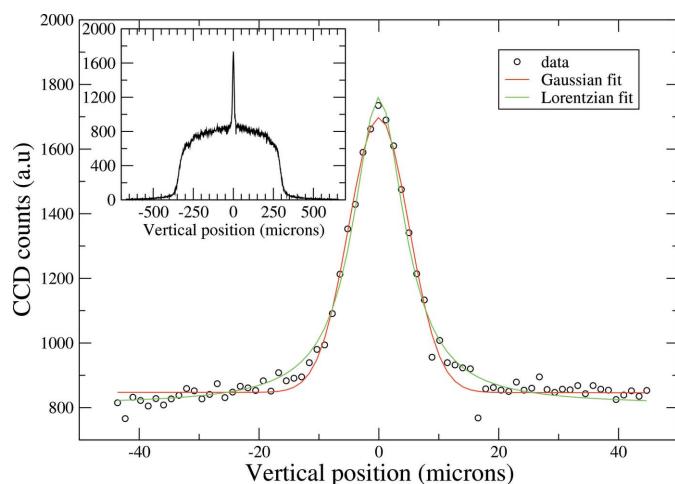


Figure 5
Measured focal spot size, with Gaussian and Lorentzian fits for the peak of the undulator spectrum set to 6.1 keV. The inset shows that the focal spot is centered on a high-energy pedestal that is about 650 μm wide.

energy around the calculated focal energy and selecting the energy with the highest peak intensity on the CCD. The CCD exposure is 2 μs and is not saturated. As shown in the inset of Fig. 5, a focused beam is centered on a 650 μm -wide white-beam pedestal with an intensity of about 800 counts. As the higher harmonics have focal lengths much larger than the fundamental, the profile of the white-beam background comes from all the effectively unfocused high-energy harmonics.

Fig. 5 shows the data around the focused beam with a Gaussian and a Lorentzian fit with a constant background, for a signal-to-background ratio of 1.18. The FWHM of the Gaussian fit is 11.8 μm or $\sigma_{\text{ip}} = 5$ μm . The profile is fit well by a Gaussian line profile and the measured RMS focal spot size compares well with the calculations in Table 1. The Lorentzian fit shown in Fig. 5 has a higher least-squares χ^2 than the Gaussian fit, but a FWHM of 10.4 μm . The Lorentzian fit has an improved signal-to-background ratio, a smaller width and better agreement in the tail.

The measurements were repeated with $N = 6$ Be lenslets. The best focus occurred for an X-ray energy of 7.47 keV. At this energy, we find also $f = 2.72$ m, and $r_i = 2.95$ m. Fig. 6 shows the data around the focused beam with a Gaussian fit and a Lorentzian fit with a constant background. For this configuration, the best fit is a Lorentzian with a FWHM of 9.1 μm (a Gaussian fit is 10.6 μm wide). The signal-to-background ratio at this higher energy is 3.8. The measured performance is improved at higher energies with a smaller focal spot size and greater contrast. Our beamline, choppers and lens Be windows attenuate the softer X-rays with a transmission of approximately 52% at 6.1 keV and 70% at 7.47 keV. This would improve the ratio of focal spot intensity over high-energy background to 2.25 and 5.4 at 6.1 and 7.47 keV, respectively, if the windows were removed. Our model in Table 1 predicts a slightly broader width, but the approximation is reasonable considering that we assumed the source spectrum to be Gaussian whereas the asymmetry of the spectrum is clearly seen from Fig. 1.

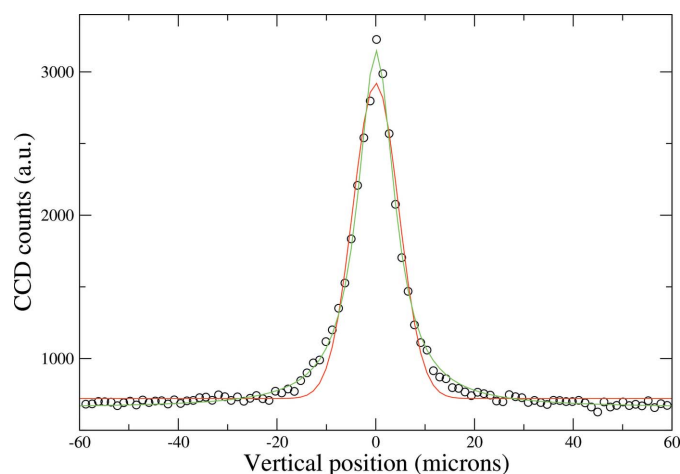


Figure 6
Measured focal spot size (circles), Gaussian fit (red line) and Lorentzian fit (green line) for the peak of the undulator spectrum set to 7.47 keV. Here the number of lenslets is $N = 6$.

Some differences remain but the simplified model provides a quick estimate of the expected spot size with pink beam which should be helpful for experimenters.

5. Discussion

The model developed here is useful for designing optical systems where the energy must be changed frequently. For ideal performance, one must obtain lenses with finely varying focal lengths. If one can tolerate chromatic aberration, then one can design with coarser sets of available focal lengths, reducing the design complexity. Note that a pneumatically actuated device called a transfocator was recently developed to insert lenslets by remote control so that one can change N as needed (Vaughan *et al.*, 2011).

The significant high-energy background to the focal profile (inset of Fig. 5) could be removed by a multilayer monochromator or a flat grazing-incidence mirror. For the EBIT signal, the K -shell fluorescence is measured with an energy-dispersive detector so this background is irrelevant for this experiment.

A CRL may be able to reduce the bandwidth of pink beam from an undulator if a slit or pinhole located in the focal plane spatially filters the focused beam to dimensions comparable with σ_i . Chromatic aberrations, as shown in equation (4), become comparable with σ_i when

$$\sigma_E/E \approx \frac{\sigma_i}{2\sigma_a} \frac{r_i(r_s - f)^2}{r_s^2 f}, \quad (5)$$

or, for simplicity, $\sigma_E/E \approx \sigma_i/(2\sigma_a)$ when $f \ll r_s$. This would result in $\sigma_E/E \approx 0.2\%$ for values taken in Table 1 at 6.1 keV. When $r_s = r_i = 2f$, $\sigma_i = \sigma_s$; thus $\sigma_E/E \approx \sigma_s/(4\sigma_a)$. Using computed numbers from Table 2 with $\sigma_a = 633 \mu\text{m}$ and $\sigma_s = 11.6 \mu\text{m}$, we find $\sigma_E/E \approx 0.46\%$. A 1:1 imaging ratio could reduce the pink beam bandwidth while making it easier to implement with a more gentle focus and smaller power density in the focal plane.

We explored the performance of a Be parabolic CRL with a pink hard X-ray beam. In an experiment with a 10:1 demagnification ratio, the focal spot size is blurred by a factor of five from the ideal image of the source, consistent with a simple model of chromatic aberration. We demonstrated a method based on X-ray choppers and a synchronized CCD camera to observe the focused pink beam without X-ray filters. Although

the aberrations are significant, a focal spot size with a FWHM below $10 \mu\text{m}$ in the vertical was possible at 7.5 keV. This may be adequate for many synchrotron imaging experiments with a broad energy bandpass up to a few percent.

Acknowledgements

The authors wish to thank Harold Gibson for technical support. This work was performed on the APS 7-ID beamline. Use of the Advanced Photon Source, an Office of Science User Facility operated for the US Department of Energy (DOE) Office of Science by Argonne National Laboratory, was supported by the US DOE under contract No. DE-AC02-06CH11357.

References

- Alianelli, L., Sánchez del Río, M. & Sawhney, K. (2007). *At. Spectrosc.* **62**, 593–597.
- Dufresne, E., Adams, B., Arms, D. A., Chollet, M., Landahl, E., Li, Y., Walko, D. A. & Wang, J. (2010). *Proceedings of SRI2009: Tenth International Conference on Radiation Instrumentation*, edited by R. Garrett, I. Gentle, K. Nugent and S. Wilkins, Vol. CP1234, pp. 181–184. Melville: American Institute of Physics.
- Gembicky, M. & Coppens, P. (2007). *J. Synchrotron Rad.* **14**, 133–137.
- Gembicky, M., Oss, D., Fuchs, R. & Coppens, P. (2005). *J. Synchrotron Rad.* **12**, 665–669.
- Lengeler, B., Schroer, C. G., Benner, B., Gerhardus, A., Günzler, T. F., Kuhlmann, M., Meyer, J. & Zimprich, C. (2002). *J. Synchrotron Rad.* **9**, 119–124.
- Moon, S., Liu, Z., Gao, J., Dufresne, E., Fezzaa, K., Wang, J., Xie, X. & Lai, M. (2010). In *Proceedings of ILASS Americas, 22nd Annual Conference on Liquid Atomization and Spray Systems*. Available at <http://www.ilass.org/2/ConferencePapers/ILASS2010-154.PDF>.
- Polikarpov, M., Snigireva, I. & Snigirev, A. (2014). *J. Synchrotron Rad.* **21**, 484–487.
- Reeves, R. V., White, J. D. E., Dufresne, E. M., Fezzaa, K., Son, S. F., Varma, A. & Mukasyan, A. S. (2009). *Phys. Rev. B*, **80**, 224103.
- Sánchez del Río, M. & Dejus, R. J. (1997). *Proc. SPIE*, **3152**, 148–157.
- Silver, E., Gillaspay, J. D., Gokhale, P., Kanter, E. P., Brickhouse, N. S., Dunford, R., Kirby, K., Lin, T., McDonald, J., Schneider, D., Seifert, S. & Young, L. (2011). *Proceedings of the Twenty First International Conference on Application of Accelerators in Research and Industry*, edited by F. D. McDaniel and B. L. Doyle, Vol. 1336, pp. 146–149. American Institute of Physics Conference Series.
- Snigirev, A., Kohn, V., Snigireva, A. & Lengeler, B. (1996). *Nature (London)*, **384**, 49–51.
- Vaughan, G. B. M., Wright, J. P., Bytchkov, A., Rossat, M., Gleyzolle, H., Snigireva, I. & Snigirev, A. (2011). *J. Synchrotron Rad.* **18**, 125–133.